HHS Public Access

Author manuscript

J Periodontal Res. Author manuscript; available in PMC 2024 August 01.

Published in final edited form as:

J Periodontal Res. 2023 August ; 58(4): 723–732. doi:10.1111/jre.13130.

The LRP5 high-bone-mass mutation causes alveolar bone accrual with minor craniofacial alteration

Hakan Turkkahraman, DDS, PhD[1], **Shannan Flanagan, BS**[2], **Tianli Zhu, MD**[3], **Teresita M. Bellido, PhD**[4], **Xue Yuan, PhD**[2,5]

[1]Indiana University School of Dentistry, Department of Orthodontics and Oral Facial Genetics, Indianapolis, IN, USA.

[2]Indiana University School of Medicine, Department of Otolaryngology-Head & Neck Surgery, Indianapolis, IN, USA.

[3]Indiana University School of Dentistry, Department of Biomedical Sciences and Comprehensive Care, Indianapolis, IN, USA.

[4]University of Arkansas for Medical Sciences, Department of Physiology and Cell Biology, Little Rock, AR, USA.

[5]Indiana University School of Medicine, Indiana Center for Musculoskeletal Health, Indianapolis, IN, USA.

Abstract

Background and objective: Mutations in low-density lipoprotein receptor-related protein 5 (LRP5) cause various bone diseases. Several mouse models were generated to study the role of LRP5 in bone development. But most of the studies were confined to the appendicular skeleton. The role of LRP5 in the axial skeleton, especially in the craniofacial skeleton, is largely unknown. The aim of this study was to investigate the craniofacial phenotype with the $LRP5_{G171V}$ mutation.

Methods: To understand how LRP5 affects craniofacial bone properties, we analyzed *LRP5* high-bone-mass mutant mice carrying the G171V missense mutation ($LRP5^{HBM}$). Quantitative micro-computed tomographic imaging and histomorphometric analyses were used to study craniofacial phenotypes and bone density. Histology, immunohistochemistry, and *in vivo* fluorochrome labeling were used to study molecular mechanisms.

Results: $LRP5^{HBM}$ mice showed overall minor changes in the craniofacial bone development but with increased bone mass in the interradicular alveolar bone, edentulous ridge, palatine bone, and premaxillary suture. Elevated osteocyte density was observed in $LRP5^{HBM}$ mice, along

Corresponding authors: Hakan Turkkahraman, DDS, PhD, 1121 West Michigan Street, Room DS249, Indianapolis, IN, 46202, Phone: (317) 278-9934, Fax: (317) 278-9933, haturk@iu.edu, Xue Yuan, PhD, 1160 West Michigan Street, GK305, Indianapolis, IN, 46202. yuanxue@iu.edu.

AUTHOR CONTRIBUTIONS

H.T., T.B., and X.Y. contributed to conception and design of the research, interpretation and wrote the paper. H.T., S.F., T.Z., T.B., and X.Y. performed the experiments, data acquisition and analysis. All authors have been involved in drafting and revising the manuscript critically and have approved the final version for publication.

CONFLICT OF INTEREST

All authors declare no conflict of interest.

with increased Runx2 expression and unmineralized bone surrounding osteocytes. Meanwhile, *LRP5*^{HBM} mice exhibited increased osteoprogenitors, but no significant changes were observed in osteoclasts. This led to a high bone mass phenotype, and an increased osteocyte density in the alveolar bone and edentulous ridge.

Conclusion: *LRP5*^{HBM} mice display increased bone mass in the alveolar bone with minor changes in the craniofacial morphology. Collectively, these data elucidated the important role of LRP5 in axial bone development and homeostasis and provided clues into the therapeutical potential of LRP5 signaling in treating alveolar bone loss.

Keywords

Wnt signaling pathway; Alveolar process; LRP5 protein; mouse; High bone mass

INTRODUCTION

The Wnt genes, initially associated with fruit fly embryo development, have been linked to a wide range of biological events and diseases, including bone development and homeostasis. Wnt signaling is complicated, with 19 ligands, 10 Frizzled receptors, 2 co-receptors, and many regulators in vertebrates. The two co-receptors are low-density lipoprotein receptor-related protein (LRP) 5 and 6.[1,2] In canonical Wnt signaling, a Wnt ligand binds to a Frizzled receptor and triggers the formation of a complex including Wnt, Frizzled, and LRP5 or LRP6, activating the Wnt pathway.[3] LRP5 and LRP6 are both single-pass transmembrane proteins. The extracellular regions of LRP5 and LRP6 interact with the Wnt antagonists Dickkopf-1 (Dkk-1) and sclerostin, while the intracellular regions interact with Axin and glycogen synthase kinase-β (GSK-β). Without LRP5 or LRP6, binding Wnt and their receptors Frizzled proteins cannot activate canonical Wnt/β-catenin signaling.[4]

The expression and activity of LRP5 also regulate Wnt signaling.[5] Mutations of LRP5 have been identified and linked to a wide variety of bone diseases, such as osteoporosis-pseudoglioma syndrome (OPPG)[6] and high bone mass.[7,8] In two unrelated high bone mass kindred, Little et al.[7] and Boyden et al.[8] identified an identical *LRP5*$_{G171V}$ mutation, in which substitution of glycine was substituted with valine at codon 171. The normal glycine lies in a propeller motif that is highly conserved from fruit flies to humans, and this single mutation leads to defective Dkk-1 signaling transduction.[8]

Mouse *LRP5*$_{V171}$ mutations recapitulated the high bone mass phenotype observed in humans. In a line carrying the human *LRP5*$_{G171V}$ complementary DNA under the expression of the 3.6 Col 1α1, the prevalence of apoptosis of osteoblasts and osteocytes was found to be decreased.[9] The mice were also reported to have increased sensitivity to load due to a lower threshold for initiating bone formation.[10,11] Cui et al.[12] introduced the *G171V* mutation into exon 3 of the mouse LRP5 gene. This strain exhibits increased bone mass, high bone mineral density, and improved biomechanical properties. These phenotypes were caused by the alerted sensitivity of LRP5 to endogenous inhibitors Dkk-1 and sclerostin.[13]

Although the bone architecture and mass/density were changed, the bone length was not affected in both human[14] and mouse models,[15] suggesting the function of LRP5 is site specific. Currently, the role of LRP5 in mediating an anabolic bone remodeling response in the appendicular skeleton has been elucidated,[11–13] but its function in the axial skeleton, especially in the craniofacial complex, is largely unknown. In this study, we set out to investigate the craniofacial phenotype with the $LRP5_{G171V}$ mutation. We found that $LRP5^{HBM}$ mice displayed slight alteration in the craniofacial morphology. However, a high bone mass phenotype was found in the interradicular alveolar bone, edentulous ridge, palatine bone, and premaxillary sutures of mutant mice. The $LRP5_{G171V}$ mutation also leads to the narrowing of the periodontal ligament (PDL) space and shifts the PDL cells to osteoprogenitors, contributing to alveolar bone formation. In both alveolar bone and edentulous ridge, mutation leads to the accumulation of Runx2+ osteocytes and unmineralized bone surrounding the osteocytes, and increased bone mass.

MATERIALS AND METHODS

Mouse

All animal procedures were performed in accordance with guidelines set by the Indiana University Institutional Animal Care and Use Committee. $LRP5_{G171V/G171V}$ ($LRP5^{HBM}$) mice were described previously.[12] The $LRP5^{HBM}$ mice were generated on a mixed 129S1/SvIMJ and C57Bl/6J background. $LRP5_{G171V}$ female mice were crossed with C57BL/6J male mice. The heterozygous mice were then crossed to generate $LRP5^{HBM}$ mice and wild-type littermate control mice. There was no significant difference in body weight between the control and $LRP5^{HBM}$ mice.[9,11,15] Five-month-old male $LRP5^{HBM}$ (n=12), and control mice (n=12) were used in this study.

Micro-computed tomographic (μCT) analyses

Heads were scanned with Skyscan 1176* under the following conditions: 59 kV X-ray energy, 9 μm pixel size, and a 0.8-degree rotation. Scanned data were reconstructed as described before.[16] Distant measurements were performed by CTan and landmarks were selected following published protocols.[17,18] The region of interests (ROI)s for volumetric analysis were as follows: alveolar bone under maxillary first molar that is composed of 9 slices on the medial of distobuccal root; alveolar bone between 2 roots of mandibular first molar composed of 12 slices; edentulous bone on medial of maxillary first molar composed of 15 slices with a 1 mm width. The cementum-enamel junction to alveolar bone crest (CEJ-ABC) distance underneath the four cusps of the maxillary second molar was measured three times and averaged.

Sample preparation and staining

After μCT scanning, samples were washed with PBS and decalcified with 0.5M EDTA (pH 7.2) for one week. Following complete demineralization, specimens were dehydrated, cleared in xylene, and infiltrated with a xylene-paraffin mixture, followed by paraffin. Six micron-thick sagittal sections were cut and collected on positively charged slides.

*Bruker, Kontich, Belgium

Sections were deparaffined and rehydrated and then stained with Hematoxylin for 4 min and washed with tap water. Sections were then differentiated with 1% acid alcohol briefly. After washing with tap water, sections were rinsed in 95% ethanol and then counterstained with Eosin Y for 15 seconds. Samples were then dehydrated through graded ethanol, cleared with xylene, and mounted with Permount.

Quantification of PDL width was performed with Image J[†]. For each group, six samples were included. For each sample, six positions around the maxillary first molar were randomly selected, and the width was measured and averaged.

Pentachrome staining was performed with the Pentachrome staining kit[‡].

Alkaline phosphatase (ALP) staining

Slides were deparaffined and pretreated with staining buffer (0.1M Tris pH 9.0, 50mM $MgCl_2$, 100mM NaCl, and 0.1% Tween 20) at 37°C for 15 min. The slides were then incubated with a 1-Step NBT/BCIP substrate solution[§] at 37°C for 1 hour. Slides were briefly washed and counterstained with 0.1% nuclear fast red.

Immunohistochemistry staining

Immunohistochemistry staining was performed as we described before.[19] Primary antibodies used in this study were anti-sclerostin**, anti-Dkk-1[††], active beta-catenin[‡‡], anti-PCNA[§§], anti-Periostin***, anti-Runx2[†††], anti-Cathepsin K[‡‡‡], and anti-osteopontin (OPN)[§§§]. Control and *LRP5*^{HBM} mutant mice sections were stained using the same concentration of antibody for the same length of time. The stained sections were photographed with identical parameters. The fluorescence intensity corresponding to sclerostin expression was counted by the histogram function in Photoshop (Version 22.5, Adobe, San Jose, USA).

In vivo fluorochrome labeling

Mice were injected intraperitoneally with Calcein (30 mg/kg) and Alizarin Red (50 mg/kg) at a seven-day interval. Samples were processed as we described before.[20] The active periosteal surface was measured by Calcein+ bone surface and total bone surface and expressed as percentage.[21] The number of active lacunae was measured by counting Calcein+ lacunae and normalized to bone area.

[†]NIH, Bethesda, ML
[‡]Electron Microscopy Sciences #26385
[§]Thermo Fisher #34042
[**]R&D, AF1589
[††]R&D, AF1765
[‡‡](Cell Signaling Protein, #8814)
[§§]Proteintech, 24036–1
[***]Proteintech, 19899–1
[†††]Santa Cruz, sc-390351
[‡‡‡]Santa Cruz, sc-48353
[§§§]Proteintech, 22952–1

Statistical analysis

Results were presented as means ± SD. Data was first tested for normal distribution with Shapiro-Wilk test. Then, groups were statistically compared with a two-tailed unpaired Student's *t* test. Prism 9**** was used for all statistical analyses. Significance was attained at $p<0.05$.

RESULTS

LRP5^{HBM} mice showed only minimal changes in the craniofacial morphology

To find out possible effects of the *LRP5*^{HBM} mutation on the overall morphology of the craniofacial bones, we first compared mandibles between control and *LRP5*^{HBM} mice using μCT. From the sagittal view (Fig. 1A, B), we measured and compared edentulous ridge height, alveolar height, ramus height, mandibular length, and corpus length (Fig. 1C). Overall, the length and the height of the mandible were preserved, while only a significant amount of increase was found at the edentulous ridge height, which was possibly due to appositional bone formation (Fig. 1C). The growth of the mandible occurs mainly in the condylar area. The condylar growth did not appear to be affected by the mutation as ramus heights and mandibular length were both comparable. From the transversal view (Fig 1D, E), we measured alveolar, inter-molar and inter-condylar widths. No significant changes were observed in transverse dimensions of the mandible.

We then compared midface between control and *LRP5*^{HBM} mice. From the sagittal view, we measured the length and height of the midface (Figure 1G, H). Our measurements revealed no significant change in overall length of the midface, as well as the proportions of the premaxilla, maxilla and the palatine bone (Figure 1I). The midface height of *LRP5*^{HBM} mice was also comparable with the controls (Figure 1I). When evaluated from the axial view, a significant increase was found in the maxillary width (P<.05), while premaxillary, inter-molar and palatal widths did not show any significant change (P>.05) (Figure 1J–L).

The mass and density of the alveolar bone were increased in *LRP5*^{HBM} mice

After our initial analyses of the gross morphology of the craniofacial bones, we compared the mass and density of the maxillary and mandibular bones. First, we examined the interradicular alveolar bone in the mandible (Fig. 2A, B) and found that *LRP5*^{HBM} mice had a significantly higher bone volume and denser bone (Fig. 2C, D, quantified in E). We also examined the maxillary 1st molar interradicular alveolar bone. Here, the bone was remarkably thicker in *LRP5*^{HBM} mice (Fig. 2F, G). *LRP5*^{HBM} mice displayed higher bone volume and denser bone (Fig. 2H, I, quantified in J). Then, we questioned whether this effect was site-specific and under the influence of the dentition. Therefore, we examined the mandibular corpus by examining the coronal section of the mandible. μCT results demonstrated overgrowth of mandibular bone in *LRP5*^{HBM} mice (Supplemental Fig. 1A, B, quantified in C). Histological sections of mandibles confirmed thickened cortical bone in *LRP5*^{HBM} mice (Supplemental Fig. 1D, E). Notably, in *LRP5*^{HBM} mice, the vascular space was dramatically reduced (Supplemental Fig. 1A, B, D, E) with active bone formation

****GraphPad Software, La Jolla, CA, USA

(Supplemental Fig. 1D‘, E‘). We also compared the quality of the bone on the buccal side of the maxillary first molar (Supplemental Fig. 2A, B). Similarly, *LRP5*^{HBM} mice showed increased bone mass (Supplemental Fig. 2C). Interestingly, the CEJ-ABC was comparable between control and *LRP5*^{HBM} mice (Supplemental Fig. 2D).

In addition to the alveolar bone, we also found the thickness of the palatine bone increased in *LRP5*^{HBM} mice (Supplemental Fig. 3A, B). *LRP5*^{HBM} mice also displayed abnormal premaxillary suture patterns (Supplemental Fig. 4A–F), with more space occupied by bone tissue instead of fibrous connective tissue (Supplemental Fig. 4G). However, the length of the premaxilla was comparable between control and *LRP5*^{HBM} mice (Fig. 1I).

Osteocyte density and lacunar turnover are increased in *LRP5*^{HBM} mice

Since *LRP5*^{HBM} mice recaptured the high bone mass phenotype, we then attempted to determine the underlying mechanism. We observed that the osteocyte density was considerably increased in the alveolar bone under the maxillary first molar in *LRP5*^{HBM} mice (Fig. 3A–C). ALP staining confirmed that bone formation activity was elevated in the alveolar bone of *LRP5*^{HBM} mice (Fig. 3D, E). By Pentachrome staining, we found some of the osteocytes were surrounded by osteoid, demonstrating unmineralized bone (Fig. 3F, G). Runx2 is crucial for immature osteoblasts, but its expression fades as osteoblasts and osteocytes mature[22]. This was evidenced in the control group (Fig. 3H). But we observed some Runx2+ osteocytes in the *LRP5*^{HBM} group (Fig. 3I). These cells were trapped in the bone matrix and actively expressed sclerostin and Dkk-1 (Fig. 3J–N), suggesting they are mature osteocytes.

PDL favors alveolar bone osteogenesis in *LRP5*^{HBM} mice

Optimum PDL space is necessary for the function and homeostasis of the PDL[23]. PDL space was narrowed in *LRP5*^{HBM} mice (Fig. 4A–E), but no evidence of ankylosis was detected. Periostin was normally expressed in the PDL (Fig. 4F, G) and PDL fiber alignment was maintained (Fig. 4H, I) in *LRP5*^{HBM} mice. These data suggest that, except for the narrowed PDL space, the PDL was healthy in *LRP5*^{HBM} mice. Osteoprogenitor cells exist in the PDL and contribute to alveolar bone formation and remodeling.[24,25] ALP staining and OPN staining demonstrated that bone formation activity was elevated in the PDL in *LRP5*^{HBM} mice (Fig. 4J–M). Immunostaining of active beta-catenin uncovered Wnt activated cells on the alveolar bone surface in *LRP5*^{HBM} mice (Fig. 4N,O). There were osteogenic cells as evidenced by Runx2 expression (Fig. 4P, Q). These data indicate that in *LRP5*^{HBM} mice, elevated Wnt signaling in the PDL space promotes bone formation, contributing to the high bone mass phenotype.

PDL cells are usually not mitotically active cells in homeostasis (Fig. 4R). Interestingly, we observed an increase in the number of proliferating cells in the PDL of *LRP5*^{HBM} mice (Fig. 4S). This suggests that in *LRP5*^{HBM} mice, osteoprogenitors may proliferate more before they differentiate to osteoblasts. In this way, more osteoblasts existed in the PDL in *LRP5*^{HBM} mice, producing more bone. We also examined osteoclasts. Comparable osteoclasts were found in both groups (Fig. 4T, U, T’, U’), indicating the high bone mass was not due to a deficiency in bone resorption.

Increase in maxillary edentulous ridge bone mass of *LRP5^{HBM}* mice

The edentulous ridge is composed of dense lamellar bone, which is different from the alveolar bone surrounding the teeth.[26] We discovered that the maxillary edentulous ridge in *LRP5^{HBM}* mice was thicker in both height (Fig. 5A, B, quantified in E) and width (Fig. 5C, D). The total edentulous ridge bone volume in *LRP5^{HBM}* mice was significantly larger than that in control mice (Fig. 5E). The majority of osteocytes in the control group were spindle-shaped and parallel to the bone (Fig. 5F), but in the *LRP5^{HBM}* group, some of the osteocytes were spindle-shaped and others were round (Fig. 5G). We also found newly produced osteoid in the edentulous ridge bone (Fig. 4H, I, H', I'). Runx2+ osteocytes were observed in the *LRP5^{HBM}* group (Fig. 5J, K). These cells expressed sclerostin (Fig. 5L, M). We observed fluorochrome labeling in bone surrounding osteocytes within the edentulous ridge bone (Fig. 5N, O, quantified in P), demonstrating bone apposition. Although both groups showed active mineralization at the periosteal surface, a higher portion of this actively mineralizing surface was observed in the *LRP5^{HBM}* group (Fig. 5N–P). The cell density in the periosteum as well as the thickness of the periosteum seems unchanged in *LRP5^{HBM}* mice (Fig. 5Q, R). But osteoprogenitors in the periosteum increased as evidenced by Runx2 staining (Fig. 5S, T), which may directly contribute to the increased osteocytes in the edentulous ridge bone. Taking these together, we conclude that with the *LRP5^{HBM}* mutation, increased osteoprogenitors contribute to the high bone mass phenotype and meanwhile osteocytes undergo the maturation process without ceasing Runx2 expression.

DISCUSSION

Patients with LRP5G171V mutation showed a thickened mandible and torus palatinus in addition to the high bone mass phenotype in long bone.[8] In our study, *LRP5^{HBM}* mice recapitulate the high bone mass without causing major changes in the craniofacial phenotype. We attribute these phenotypes to increased osteoprogenitors in the PDL as well as the periosteum. In the presence of the *LRP5^{HBM}* mutation, mice displayed higher osteocyte density and their osteocytes retained Runx2 expression.

Multi-scale control Wnt in the craniofacial development

We previously examined the craniofacial phenotype of several transgenic lines manipulating Wnt signaling in different ways. For example, we found that sclerostin deletion (*Sost$^{-/-}$*) increased the appositional bone growth, resulting in enlarged mandibles.[27] *Sost$^{-/-}$* mice also displayed increased bone mass in the maxillary alveolar bone and edentulous ridge,[27] similar to what we found in this study with *LRP5^{HBM}* mice. Although both *Sost$^{-/-}$* mice and *LRP5^{HBM}* mice showed similar phenotypes in the premaxillary suture, only *Sost$^{-/-}$* mice displayed significantly shortened faces.[27] The milder phenotype observed in *LRP5^{HBM}* mice suggested that sclerostin may function earlier in the developmental process compared with LRP5. Although sclerostin needs to bind LRPs to negatively regulate Wnt signaling, they may have different spatial and temporal expression patterns during craniofacial development, resulting in varied Wnt signaling status.

We have also examined the craniofacial development of a transgenic strain which has activated β-catenin in dmp1-expressing cells (*daβcat^{Ot}*).[28,29] In addition to maxillary

and mandibular hyperostosis, premaxillary sutures in *daβcat*^{Ot} mice were fused with significantly shorter but wider faces.[28] *Daβcat*^{Ot} mice also exhibited severe defects in the periodontium with calcified PDL and ankylosed teeth.[29] We only observed mild narrowing of PDL spaces in *LRP5*^{HBM} mice. *Sost*$^{-/-}$ mice exhibit no significant periodontium-related defects.[27] It is not surprising that *daβcat*^{Ot} mice have the most severe phenotypes among these three strains, as β-catenin is the effector of all components of the Wnt signaling pathway. For *Sost*$^{-/-}$ and *LRP5*^{HBM} mutations, there might be Dkks and LRP6 that compensate for the function to some degree. Future work is warranted to further clarify the role of LRP5 in craniofacial tissues.

PDL width is controlled by Wnt signaling

Maintaining PDL width is essential for the homeostasis and functionality of the tissue. We found that osteogenic activity increased in the PDL space in *LRP5*^{HBM} mice, resulting in the narrowing of the PDL spaces. Lim et al. reported that mice with overexpression of *LRP5*$_{G171V}$ showed significant narrowing of the PDL space, accompanied by increased osteogenic cells and reduced bone resorption activity.[23] We did not observe any effects in osteoclasts. We reasoned that the approaches for the two strains differ. Lim et al. used the transgenic overexpression approach. These mice harbor a transgene coding for the human *LRP5*$_{G171V}$ mutation, driven by a 3.6 kb fragment of the rat 3.6 Col 1α1 promoter. In our study, mice were knocked-in the *G171V* missense mutation into the endogenous LRP5 sequence. These mice express the HBM mutant receptors at normal levels due to the retention of the endogenous LRP5 promoter driving transcription. Overexpression of LRP5/6 ectopically activates Wnt signaling.[30] Therefore, the difference in bone resorption may result from different levels of *LRP5*$_{G171V}$ expression.

When the PDL width cannot be maintained, ankylosis ensues. This happens in *Daβcat*^{Ot} mice,[29] thus Wnt signaling must be repressed in the PDL space to main the fibrous nature. We previously found that Wnt-responsive cells exist in the PDL and slowly renew the tissue,[25] indicating that Wnt signaling needs to be precisely controlled in the PDL. When Wnt signaling is abnormally increased in the PDL, it will disrupt homeostasis and favor bone formation, as we observed in *LRP5*^{HBM} and *Daβcat*^{Ot} mice.

Wnt signaling and osteocyte maturation

The density of osteocytes was significantly increased in the alveolar bone of *LRP5*^{HBM} mice. It is possible that in *LRP5*^{HBM} mice, osteoblast apoptosis was suppressed; thus, more osteoblasts were embedded in bone and became osteocytes. Indeed, LRP5 was found to be associated with osteoblast apoptosis.[31] *Daβcat*^{Ot} mice also showed increased osteocyte density,[28] suggesting this effect is Wnt dependent. However, osteocyte density in maxillary bone was unchanged in *Sost*$^{-/-}$ mice compared with control mice.[27] The number of osteoblasts increased in *Sost*$^{-/-}$ mice with enhanced extracellular matrix secretion rate. These findings suggest Wnt signaling controls osteocyte density through LRP5, but this effect is sclerostin independent.

We found that osteocytes in *LRP5*^{HBM} mice expressed Runx2. In fact, Runx2+ osteocytes were observed in *Daβcat*^{Ot} mice but not in *Sost*$^{-/-}$ mice.[27,28] These data suggested that

LRP5 is a key player to regulate Wnt signaling during osteocyte maturation. Constitutively activated Wnt signaling increases the transition rate of osteoblasts to osteocytes and retained Runx2 expression.

Limitations

One limitation of this study was that only male mice were used. Further studies, including female mice, are needed to determine if the findings presented in this study can be generalized to both sexes. Another limitation is that LRP5 is also known to have functions in the liver and kidney,[32,33] which could affect bone metabolism. However, in this study, we did not analyze these organs. Therefore, it is unclear whether the observed effects on bone are solely due to LRP5 regulation in bone cells or if there are other factors at play. Further research is required to fully understand the role of LRP5 on the craniofacial bone homeostasis.

Clinical implications

The Wnt pathway is an attractive therapeutic target that directly promotes bone growth and regeneration. However, exaggerated activation of Wnt in craniofacial bone may cause adverse effects, as we have seen in $Da\beta cat^{Ot}$ mice. Osteoblasts in $Da\beta cat^{Ot}$ mice produce significantly more matrix, but bone quality suffers as a consequence of the high rate of bone deposition.[28] In addition, $Da\beta cat^{Ot}$ mice endure cementum overgrowth and dental ankylosis.[29] In contrast, $LRP5^{HMB}$ mice exhibited a strong bone mass increase without obvious side effects. Therefore, therapies with the ability to mimic $LRP5^{HMB}$ activation could be an effective strategy to treat bone disorders, such as progressive alveolar bone loss in periodontitis.

Conclusion

$LRP5^{HBM}$ mice display increased bone mass in the alveolar bone with minor changes in the craniofacial morphology. Increased osteoprogenitors contribute to the high bone mass phenotype while osteocytes undergo the maturation process without ceasing Runx2 expression. Collectively, these data elucidated the important role of LRP5 in axial bone development and homeostasis and provided clues into the therapeutical potential of LRP5 signaling in treating alveolar bone loss.

Supplementary Material

Refer to Web version on PubMed Central for supplementary material.

ACKNOWLEDGMENTS

We thank Dr. Mizuho Kittaka for the help of μCT analysis. This work was supported by the National Institute of Dental and Craniofacial Research (R00DE028585 to X. Y.), Veterans Administration (I01BX002104 and IK6BX004596 to T.B.), National Institutes of Health (R01AR059357 to T.B.), Indiana University-Indiana University School of Medicine Strategic Research Initiative, Ralph W. and Grace M. Showalter Research Trust, Indiana University School of Medicine, and the University of Arkansas for Medical Sciences College of Medicine Sturgis Endowment Grant.

DATA AVAILABILITY STATEMENT

The data that support the findings of this study are available from the corresponding author upon reasonable request.

References

1. Wehrli M, Dougan ST, Caldwell K, et al. arrow encodes an LDL-receptor-related protein essential for Wingless signalling. Nature. 2000;407(6803):527–530. [PubMed: 11029006]
2. Tamai K, Semenov M, Kato Y, et al. LDL-receptor-related proteins in Wnt signal transduction. Nature. 2000;407(6803):530–535. [PubMed: 11029007]
3. Grainger S, Willert K. Mechanisms of Wnt signaling and control. Wiley Interdiscip Rev Syst Biol Med. 2018:e1422. [PubMed: 29600540]
4. Ren Q, Chen J, Liu Y. LRP5 and LRP6 in Wnt Signaling: Similarity and Divergence. Front Cell Dev Biol. 2021;9:670960. [PubMed: 34026761]
5. Westendorf JJ, Kahler RA, Schroeder TM. Wnt signaling in osteoblasts and bone diseases. Gene. 2004;341:19–39. [PubMed: 15474285]
6. Gong Y, Vikkula M, Boon L, et al. Osteoporosis-pseudoglioma syndrome, a disorder affecting skeletal strength and vision, is assigned to chromosome region 11q12–13. Am J Hum Genet. 1996;59(1):146–151. [PubMed: 8659519]
7. Little RD, Carulli JP, Del Mastro RG, et al. A mutation in the LDL receptor-related protein 5 gene results in the autosomal dominant high-bone-mass trait. Am J Hum Genet. 2002;70(1):11–19. [PubMed: 11741193]
8. Boyden LM, Mao J, Belsky J, et al. High bone density due to a mutation in LDL-receptor-related protein 5. N Engl J Med. 2002;346(20):1513–1521. [PubMed: 12015390]
9. Babij P, Zhao W, Small C, et al. High bone mass in mice expressing a mutant LRP5 gene. J Bone Miner Res. 2003;18(6):960–974. [PubMed: 12817748]
10. Robinson JA, Chatterjee-Kishore M, Yaworsky PJ, et al. Wnt/beta-catenin signaling is a normal physiological response to mechanical loading in bone. J Biol Chem. 2006;281(42):31720–31728. [PubMed: 16908522]
11. Saxon LK, Jackson BF, Sugiyama T, Lanyon LE, Price JS. Analysis of multiple bone responses to graded strains above functional levels, and to disuse, in mice in vivo show that the human Lrp5 G171V High Bone Mass mutation increases the osteogenic response to loading but that lack of Lrp5 activity reduces it. Bone. 2011;49(2):184–193. [PubMed: 21419885]
12. Cui Y, Niziolek PJ, MacDonald BT, et al. Lrp5 functions in bone to regulate bone mass. Nat Med. 2011;17(6):684–691. [PubMed: 21602802]
13. Niziolek PJ, MacDonald BT, Kedlaya R, et al. High Bone Mass-Causing Mutant LRP5 Receptors Are Resistant to Endogenous Inhibitors In Vivo. J Bone Miner Res. 2015;30(10):1822–1830. [PubMed: 25808845]
14. Johnson ML, Gong G, Kimberling W, Recker SM, Kimmel DB, Recker RB. Linkage of a gene causing high bone mass to human chromosome 11 (11q12–13). Am J Hum Genet. 1997;60(6):1326–1332. [PubMed: 9199553]
15. Akhter MP, Wells DJ, Short SJ, et al. Bone biomechanical properties in LRP5 mutant mice. Bone. 2004;35(1):162–169. [PubMed: 15207752]
16. Kittaka M, Yoshimoto T, Hoffman H, Levitan ME, Ueki Y. RANKL-independent osteoclastogenesis in the SH3BP2 cherubism mice. Bone Rep. 2020;12:100258. [PubMed: 32258251]
17. Nakamura A, Zeredo JL, Utsumi D, Fujishita A, Koga Y, Yoshida N. Influence of malocclusion on the development of masticatory function and mandibular growth. Angle Orthod. 2013;83(5):749–757. [PubMed: 23327417]
18. Vora SR, Camci ED, Cox TC. Postnatal Ontogeny of the Cranial Base and Craniofacial Skeleton in Male C57BL/6J Mice: A Reference Standard for Quantitative Analysis. Front Physiol. 2015;6:417. [PubMed: 26793119]

19. Yuan X, Pei X, Chen J, Zhao Y, Brunski JB, Helms JA. Comparative analyses of the soft tissue interfaces around teeth and implants: Insights from a pre-clinical implant model. J Clin Periodontol. 2021;48(5):745–753. [PubMed: 33713489]
20. Yuan X, Amin V, Zhu T, et al. Type I diabetes mellitus leads to gingivitis and an early compensatory increase in bone remodeling. J Periodontol. 2022.
21. Zhao W, Byrne MH, Wang Y, Krane SM. Osteocyte and osteoblast apoptosis and excessive bone deposition accompany failure of collagenase cleavage of collagen. J Clin Invest. 2000;106(8):941–949. [PubMed: 11032854]
22. Kim WJ, Shin HL, Kim BS, Kim HJ, Ryoo HM. RUNX2-modifying enzymes: therapeutic targets for bone diseases. Exp Mol Med. 2020;52(8):1178–1184. [PubMed: 32788656]
23. Lim WH, Liu B, Mah SJ, Yin X, Helms JA. Alveolar bone turnover and periodontal ligament width are controlled by Wnt. J Periodontol. 2015;86(2):319–326. [PubMed: 25345341]
24. Ren Y, Han X, Ho SP, et al. Removal of SOST or blocking its product sclerostin rescues defects in the periodontitis mouse model. FASEB J. 2015;29(7):2702–2711. [PubMed: 25757567]
25. Yuan X, Pei X, Zhao Y, Tulu US, Liu B, Helms JA. A Wnt-Responsive PDL Population Effectuates Extraction Socket Healing. J Dent Res. 2018;97(7):803–809. [PubMed: 29420105]
26. Li J, Yin X, Huang L, et al. Relationships among Bone Quality, Implant Osseointegration, and Wnt Signaling. J Dent Res. 2017;96(7):822–831. [PubMed: 28571512]
27. Chen J, Yuan X, Pilawski I, et al. Molecular Basis for Craniofacial Phenotypes Caused by Sclerostin Deletion. J Dent Res. 2021;100(3):310–317. [PubMed: 33078679]
28. Chen J, Cuevas PL, Dworan JS, et al. Wnt/beta-catenin Signaling Controls Maxillofacial Hyperostosis. J Dent Res. 2022;101(7):793–801. [PubMed: 35114849]
29. Wu Y, Yuan X, Perez KC, et al. Aberrantly elevated Wnt signaling is responsible for cementum overgrowth and dental ankylosis. Bone. 2019;122:176–183. [PubMed: 30408613]
30. Mao J, Wang J, Liu B, et al. Low-density lipoprotein receptor-related protein-5 binds to Axin and regulates the canonical Wnt signaling pathway. Mol Cell. 2001;7(4):801–809. [PubMed: 11336703]
31. Javaheri B, Sunters A, Zaman G, et al. Lrp5 is not required for the proliferative response of osteoblasts to strain but regulates proliferation and apoptosis in a cell autonomous manner. PLoS One. 2012;7(5):e35726. [PubMed: 22567110]
32. Hey PJ, Twells RC, Phillips MS, et al. Cloning of a novel member of the low-density lipoprotein receptor family. Gene. 1998;216(1):103–111. [PubMed: 9714764]
33. Cnossen WR, te Morsche RH, Hoischen A, et al. LRP5 variants may contribute to ADPKD. Eur J Hum Genet. 2016;24(2):237–242. [PubMed: 25920554]

Key findings:

LRP5^{HBM} mice showed overall minor changes in the craniofacial bone development but with increased bone mass in the interradicular alveolar bone, edentulous ridge, palatine bone, and premaxillary suture.

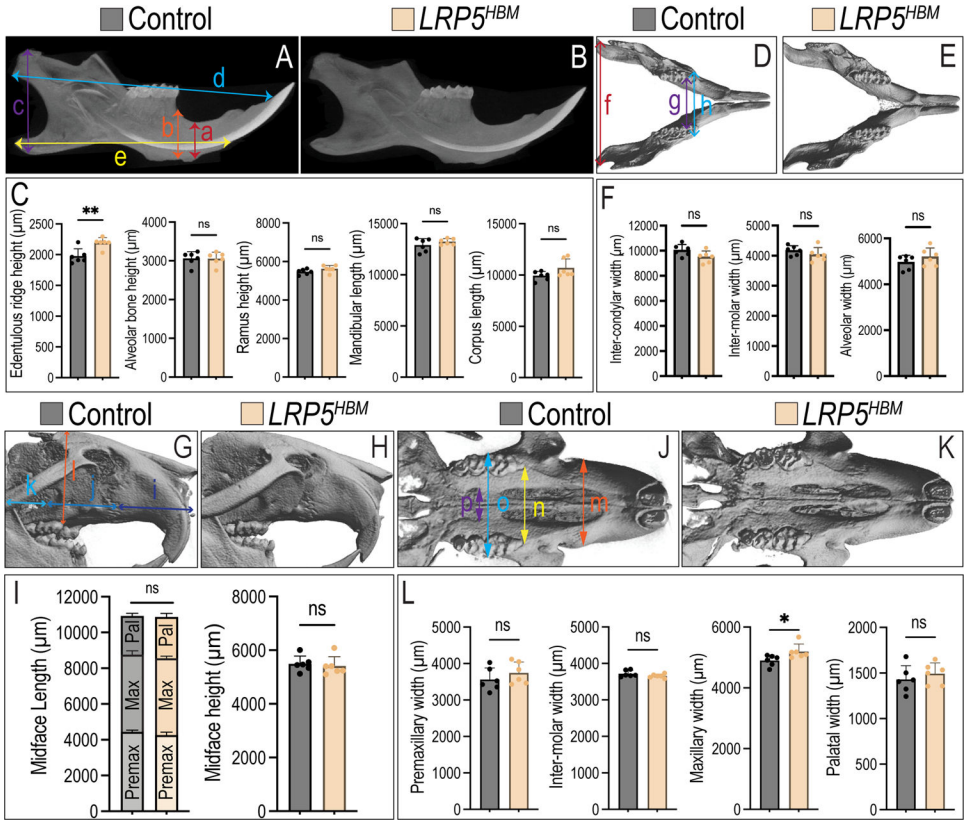

Figure 1. Craniofacial phenotypes in *LRP5*^{HBM} mice.

(A, B) Representative μCT projection images of mandibles. (C) Quantification of edentulous ridge height (a), alveolar bone height (b), ramus height (c), mandibular length (d), and corpus length (e). (D, E) Representative 3D μCT reconstruction images of mandibles. (F) Quantification of inter-condylar width (f), inter-molar width (g), and alveolar width (h). (G, H) Representative 3D μCT reconstruction images of skulls. (I) Quantification of premaxillary length (i), maxillary length (j), palatal length (k), and midface height (l). (J, K) Representative 3D μCT reconstruction images of maxillae. (L) Quantification of premaxillary width (m), inter-molar width (n), maxillary width (o), and palatal width (p). * P<0.05; ** P<0.01; ns, no significant.

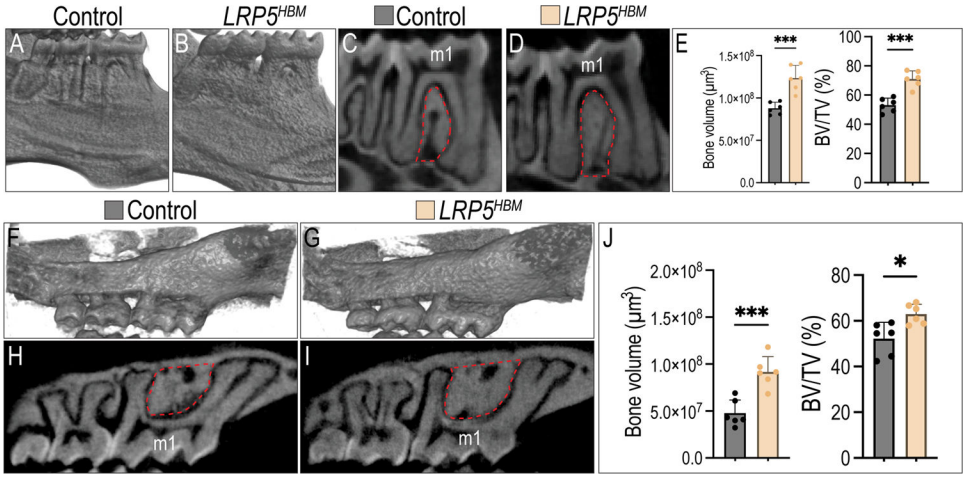

Figure 2. Alveolar bone overgrowth in *LRP5*^{HBM} mice.

(A, B) Representative 3D μCT reconstruction images of mandibular molars. (C, D) Representative sagittal 2D μCT sections of the mandibular first molars. Red dotted lines indicate the ROI for quantification. (E) Quantification of bone volume (BV) and BV/ tissue volume (TV). (F, G) Representative 3D μCT reconstruction images of maxillae. (H, I) Representative sagittal 2D μCT sections of the maxillae. Red dotted lines indicate the ROI for quantification. (J) Quantification of BV and BV/TV. Abbreviation: m1, first molar. * P<0.05; *** P<0.001.

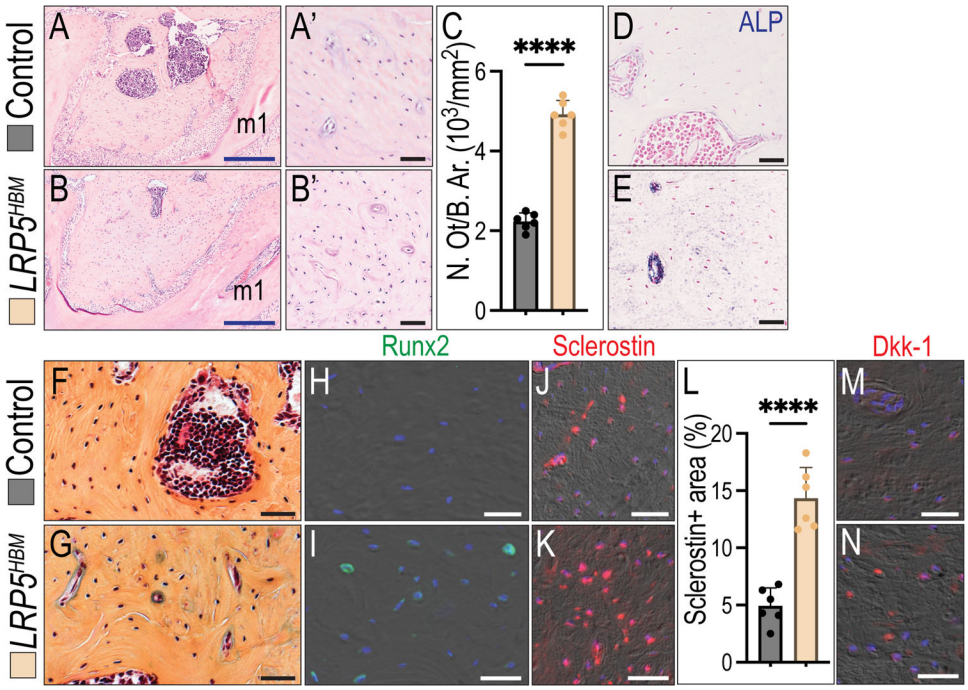

Figure 3. Osteocyte density and lacunar turnover are increased in *LRP5*^{HBM}

(A, B) H&E staining of maxillary first molars. (A', B') Higher magnification images showing the alveolar bone in the furcation areas. (C) Quantification of osteocyte density in the alveolar bone in the furcation area. (D, E) ALP staining showing the bone formation activity in the alveolar bone in the furcation area. (F, G) Pentachrome staining showing the alveolar bone in the furcation area. The yellow color represents the minimized bone while the green color represents the osteoid. Immunostaining of (H, I) Runx2, (J, K) sclerostin in the alveolar bone from the furcation area. (L) Quantification of sclerostin expression. (M, N) Dkk-1 in the alveolar bone from the furcation area. Abbreviation: m1, first molar. Scale bars: 50 μm (black) and 0.5 mm (blue). **** P<0.0001.

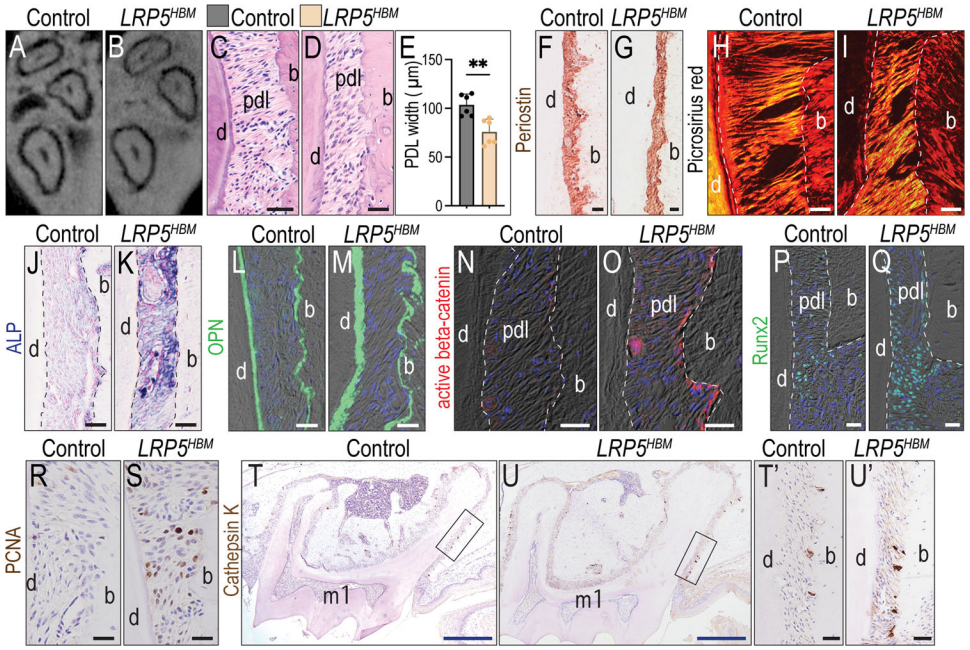

Figure 4. PDL favors alveolar bone osteogenesis in *LRP5*^{HBM} mice.

(A, B) Representative transverse 2D μCT sections of the roots from the maxillary first molar. (C, D) Representative H&E-stained histological sections of the PDL from the maxillary first molar. (E) Quantification of the PDL width. (F, G) Immunostaining of periostin. (H, I) Representative picrosirus red-stained histological sections of the PDL. The tissue was viewed under polarized light to visualize collagen fiber. (J, K) ALP staining of the PDL surrounding the maxillary first molar. Immunostaining of (L, M) osteopontin (OPN), (N, O) active beta-catenin, (P, Q) RUNX2, and (R, S) PCNA. (T, U) Immunostaining of cathepsin K. (T', U') Enlarged images of the boxes in T and U. Abbreviation: m1, first molar; d, dentin; pdl, periodontal ligament; b, bone. Scale bars: 50 μm (black) and 0.5 mm (blue). ** P<0.01.

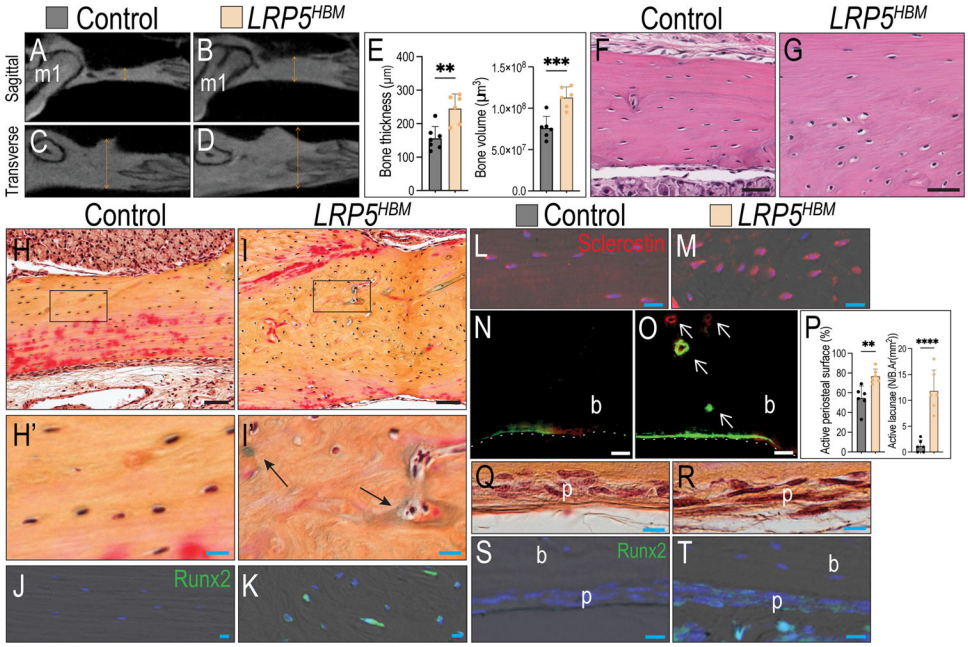

Figure 5. Increase in maxillary edentulous ridge bone mass of *LRP5*^{HBM} mice.

(A, B) Representative sagittal 2D μCT sections through the maxillary edentulous ridge. (C, D) Representative transverse 2D μCT sections through the maxillary edentulous ridge. (E) Quantification of edentulous ridge thickness and bone volume. (F, G) H&E staining and (H, I) Pentachrome staining of representative sagittal sections through the maxillary edentulous ridge. (H', I') Higher magnification images of the black box area in H and I. Arrows indicate the osteoid stained with a green color. Immunostaining of (J, K) Runx2 and (L, M) SOST. (N, O) Representative sections of calcein green- and alizarin red-labeled bone in the maxillary edentulous ridges. (P) Quantification of the active (Calcein+) periosteal surface and the number of active lacunae (Calcein+). (Q, R) Higher magnification images of the periosteum area from the Pentachrome stained slides. (S, T) Immunostaining of Runx2 in the periosteum area. Abbreviation: b, bone; m1, first molar; p, periosteum. Scale bars: 50 μm (black) and 10 μm (blue). ** P<0.01, *** P<0.001, **** P<0.0001.